Design and Investigation of TiO_2–SiO_2 Thin Films on AISI 316L Stainless Steel for Tribological Properties and Corrosion Protection

B. Shayegh Boroujeny[a,*]

a Department of Engineering, Shahrekord University, Shahrekord, Iran.

ARTICLE INFO

ABSTRACT

The TiO_2–SiO_2 thin films were deposited on the AISI 316L stainless steel via the sol-gel method. Then, the effect of the added amount of SiO_2 on the structure, morphology and mechanical properties of the films and corrosion behavior of the AISI 316L stainless steel substrate were investigated Bu using X-ray diffraction, field-emission scanning electron microscopy, atomic force microscopy, depth-sensing indentation technique supporting micro-scratch mode and potentiodynamic polarization test. It was observed that the appropriate amount of SiO_2 addition to the TiO_2 film not only decreased the particle size of the TiO_2–SiO_2 crystal but also could help to improve the surface quality. Mechanical and tribological properties of the films were found to be improved in the range of 10–15% mol of SiO_2 addition compared with the pure TiO_2. The minimum root mean square value was obtained from the film with a silica content of 10% mol. In addition, the corrosion behavior of the AISI 316L stainless steel was improved by adding 15% mol of SiO_2. Under the UV illumination conditions, photo-generated electrons accumulated in this film could perfectly protect the substrate photocathodically.

1. Introduction

Ceramic coatings on metal substrate have been essentially studied for their oxidation resistance and their applications for corrosion protection [1-4]. TiO_2–SiO_2, as a ceramic coating, has already attracted much attention in recent years not only for its possible applications in corrosion protection of the carbon steel [5-7] but also for its uses in photocatalysis [8-10] and self-cleaning [11-12]. In addition, TiO_2–SiO_2 nano-composites can be used as very interesting glass materials with ultra-low thermal expansion coefficients and high refractive indices [13-14]. Such advanced materials are naturally expected to include the properties of both phases including corrosion protection, high thermal stability and excellent mechanical strength as the properties of SiO_2 and chemical stability and higher coefficient of thermal expansion as the properties of TiO_2. Furthermore, the TiO_2–SiO_2 mixed oxides extend their uses through the production of new catalytic active sites due to the interaction of TiO_2 with SiO_2 [15]. Austenitic stainless steel, especially AISI 316L, has been extensively and

Corresponding author:
E-mail address: b.shayegh@eng.sku.ac.ir (Behrooz Shayegh Boroujeny).

used in the production of medical devices body implants owing to its good corrosion resistance and biocompatibility [16-17]. However, very few efforts have been made to apply TiO_2–SiO_2 to metallic alloys especially to the family of stainless steel for tribological and anti-corrosion applications. In our previous work [12], we investigated the photocatalytic activity of the TiO_2–SiO_2 thin films coated on AISI 316L. It was observed that the photocatalytic activity, the super-hydrophilicity and the self-cleaning properties of the films could be improved by adding SiO_2 to TiO_2. As a semiconductor under normal conditions, TiO2 absorbs light with energy equal to or greater than its band gap energy resulting in excited charge carriers: an electron, e-, and a hole, h+. The SiO_2 addition to the TiO_2 matrix increases its band gap from 3.2 to 4.5 eV [18]. As pointed out by Lassaletta et al. [19-20], the increase in the band-gap energy could be attributed to a combination of the quantum-size effect and the interface interaction due to the support effect with the support effect probably being the most important parameter. The oxidizing potential of the photo-generated holes (h+) and the reducing potential of the photo-generated electrons (e-) will increase as band-gap is increased [18]. As a result, the addition of SiO_2 to TiO_2 can improve its photocatalytic activity and increase its photo-generated electrons. On the other hand, it is well known that long thermal exposure of austenitic stainless steels to high temperatures (e.g. 700-850°C) can affect the mechanical properties of the film and the corrosion behavior of the

stainless steel. In the present work, corrosion resistance of the 316L stainless steels and the tribological and mechanical properties of the films have been studied by applying the TiO_2–SiO_2 coatings on the stainless steel surface. The present paper explains the process, which includes the deposition of the TiO_2–SiO_2 coatings with different compositions through the sol-gel method and subsequent sintering heat treatment of the coated AISI 316L stainless steel to produce a hybrid coating with good tribological and anti-corrosion properties.

2. Materials and methods
2.1. Preparation of thin films
The detailed preparation procedures for the thin films can be found in the literature [12]. An SiO_2 polymeric sol was prepared by diluting 1 mol of tetraethoxysilane (TEOS) in 2.68 ml ethanol, deionized water, and nitric acid (HNO_3). TEOS concentration in the concentrated sol was 2.35 M with a molar ratio H_2O/TEOS of 2.2, and a pH of 3.5. This solution was kept at 60°C for 2 days before use. Then 1 mol of tetraisopropylorthotitanate (TIPT) was dissolved in the solutions containing deionized water and different amounts of ethanol with the H_2O/TIPT molar ratio of 0.8 used as TIPT precursor solution. Nitric acid (HNO_3) was used for adjusting the pH to 2.5. Then TEOS and various amounts of TIPT precursor solution were mixed to obtain the concentrations listed in Table 1.

Table 1. Quantities (mol) of the products used for making the final solution used for thin film preparation

	%mol SiO_2 in composite					
	0	5	10	15	20	25
TEOS	0	0.5	0.1	0.15	0.2	0.25
TTIP	1	0.95	0.9	0.85	0.8	0.75
H_2O	0.8	0.87	0.94	1.01	1.08	1.15
EtOH	15.9	15.25	14.59	13.93	13.26	12.6

The concentration of alkoxides (TIPT + TEOS) was fixed at 0.8 M in ethanol. Before the

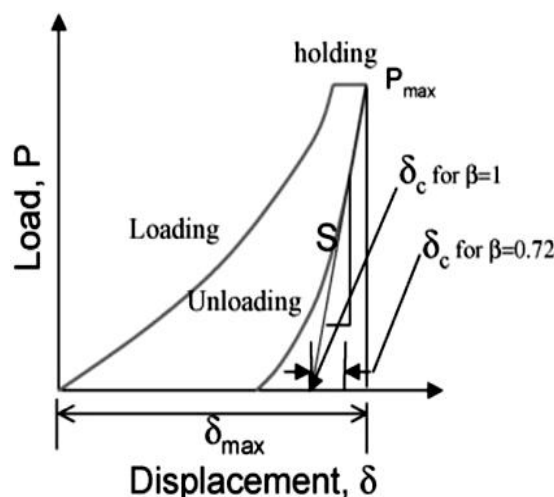application, the mixed sol was stirred for 2 h. The surfaces of the AISI 316L austenitic

Fig. 1. Schematic illustration of the load-displacement curve for an indentation

stainless steel substrate were prepared by manual grinding for different grades of SiC papers (600-1500) to produce a mirror surface. The coatings were prepared by dipping the substrates into the solution, followed by drying and then heat treating in a programmable furnace. The withdrawal rate used for preparing the films was 5 cm/min. The temperature was slowly increased (3°C /min) to 750°C and was kept at this temperature for 1 h. The film thickness was increased by repeated dipping, drying and heat-treating cycles. For all the samples three dipping cycles were repeated. The average thickness of the films was 400 nm.

2. 2. Microstructure characterization
The crystal structure of the TiO_2–SiO_2 films was studied by X-ray diffractometer (Philips PW-3040, 40kV and 30mA) using monochromatized Cu Kα radiation (λ = 0.1506 nm). The XRD spectra of the films were recorded by scanning 2θ at the range of 10–90°. The Scherrer equation was used for determining the crystallite size of the films.

2. 3. Morphological characterization
Field-emission scanning electron microscopy (FE-SEM, Hitachi 4160, 25kV) and atomic force microscopy (AFM) were used to examine the surface morphology and grain structure of the coatings.

2. 4. Mechanical properties characterization
The hardness and elastic modulus of the coatings were evaluated by depth-sensing indentation, a relatively new technique, which has been recently used to investigate the mechanical properties of the thin films. In a depth-sensing indentation test, a diamond tip is indented into the surface of the films and then the corresponding force-displacement curve, which is usually composed of loading, holding, and unloading segments, is traced as Fig.1. In Fig. 1, S is the contact stiffness between the tip and the sample and is determined as the slope of the upper portion of the unloading curve, δ_C is the contact depth, and δ_{max} is the maximum depth. Generally, the modified Oliver and Pharr's method [21] is used to analyze the indentation force–displacement curve and to calibrate the machine compliance and the indenter tip area function.

Based on this standard analysis, the reduced modulus (Er) is related to S according to the following relationship:

$$E_r = S / 2\sqrt{\pi / A} \qquad [1]$$

Where A is the contact area between the tip and coating. Then, the coating modulus (Es) can be calculated from Er by equation (2):

$$1 / E_r = \left(1 - \upsilon_s^2\right) / E_s + \left(1 - \upsilon_i^2\right) / E_i \qquad [2]$$

Where υ is the Poisson ratio, and subscripts s and i refer to sample and indenter, respectively. The hardness (H) of a sample is defined as:

$$H = P_{max} / A \qquad [3]$$

Where P_{max} is the peak indentation load.

The micro-scratch mode of the Nanotest machine using a Berkovich diamond indenter was adopted to determine the adhesion strength of the coating to the substrate. The test involved drawing the indenter over the coating surface at a constant traveling speed and at a continuously increasing load.

2. 5. Electrochemical behavior characterization

The corrosion behavior of the specimens was tested in an electrolyte of 3%wt NaCl solution using an Auto lab PGSTAT 30 Electrochemical Measurement System. The electrochemical corrosion test was carried out in a flat cell with the specimen-exposed area of 1 cm². The flat cell included a stainless steel auxiliary electrode, a saturated calomel reference electrode (SCE) and the specimens as working electrodes. The scans were carried out at a rate of 0.1 mV/ sec from – 0.25 V to +0.25 V relative to the open-circuit potential. The TiO_2– SiO_2 coated AISI 316L stainless steel samples were placed in darkness before measurements.

A 20 W black light bulb was used as a UV light source.

3. Results and discussion
3. 1. Microstructure of the films

Fig. 2 shows the XRD patterns of silica-embedded titania films that were heat-treated at 750 °C, with an inset showing the crystallite size changes of anatase phase in these films. As is evident in Fig. 2, in the XRD pattern of pure both anatase (2θ = 25.2°) and rutile (2θ = 27.5°) phases existed in the structure of the film. The rutile phase disappeared when the silica percentage exceeded 10%mol. The peaks gradually broadened as SiO_2 was added. Therefore, the crystallite size of anatase decreased when silica content of the films increased.

The anatase phase has a tetragonal unit cell and the lattice parameters (a, c) which can be determined from the peak positions (004) and (200) by the relations a = b = $2 \times d_{200}$ and c = $4 \times d_{400}$. The lattice parameters calculated for the films are shown in Table 2.
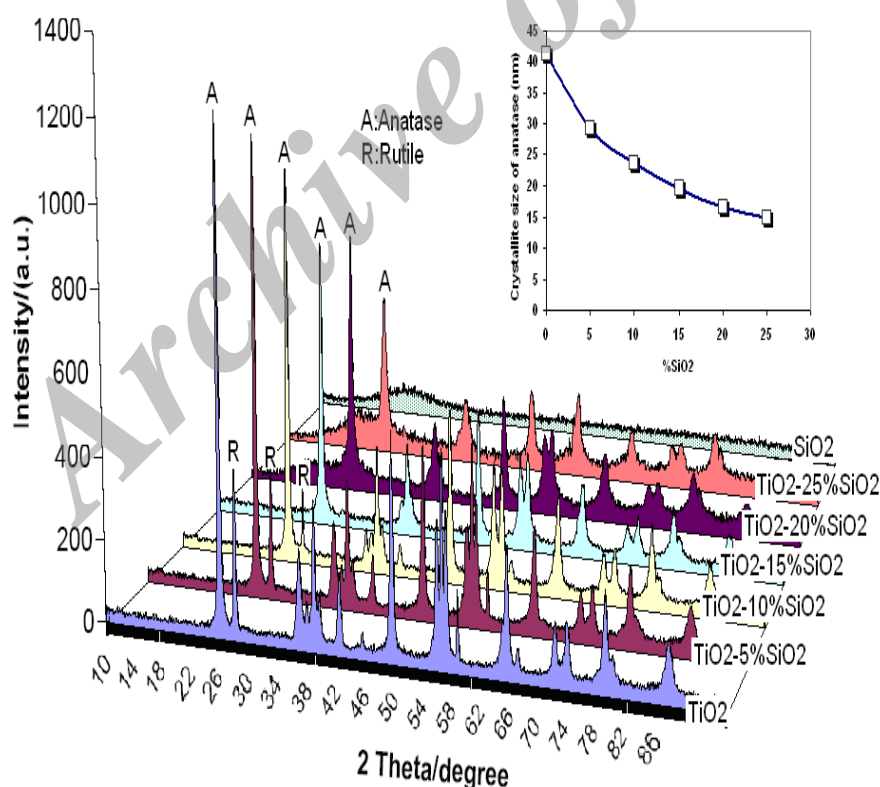

Fig. 2. XRD patterns of silica-embedded titania films heat-treated at 750°C. Inset shows effect of the silica content on the crystallite size of anatase

Table 2. The lattice parameters calculated for the films

Silica content (%mol)	Lattice parameter (a)(°A)	Lattice parameter (c)(°A)	Ratio of lattice constants(c/a)
0	3.7822	9.5007	2.5121
5	3.7811	9.4901	2.5099
10	3.7852	9.4878	2.5066
15	3.7851	9.4884	2.5068
20	3.7912	9.4655	2.4967
25	3.7958	9.4574	2.4915
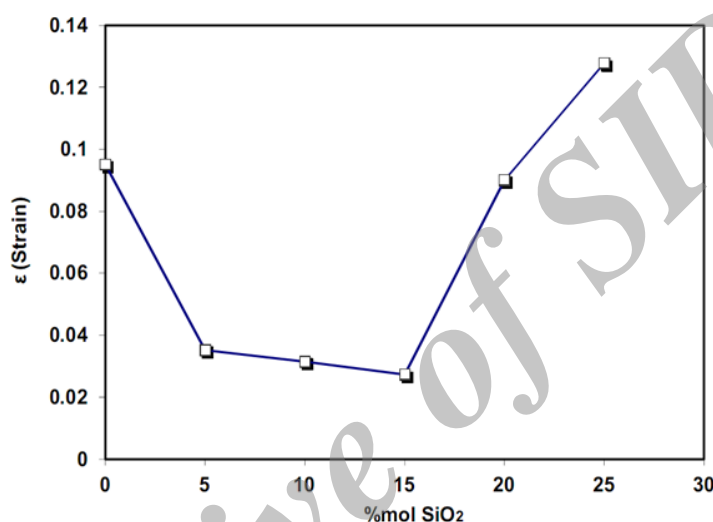
Fig. 3. The variation of the residual strain with the films silica content

Among these data, the lattice parameters calculated for the films containing 10-15%mol SiO_2 were close to the reported bulk values of the anatase phase (a = 3.7842 °A, c = 9.5146 °A) [22]. It was observed that the lattice constant a decreased with the silica percentage, whereas the lattice constant c increased. It can also be seen from Table 2 that all films were under tensile strain since the ratio of the lattice constants c/a was lower than the c/a ratio (2.5142) of the stress free TiO_2 [22]. Equation (4) shows the relationship between the FWHM (β) and residual strain [24]:

$$\beta.\mathrm{Cos}\,\theta = k\lambda / D + 4\varepsilon.\mathrm{Sin}\,\theta \qquad [4]$$

The strain ε was estimated from the slope of the plot $\beta\ \mathrm{Cos}\theta$ versus $\mathrm{Sin}\theta$. The variation of the strain with the films silica content is shown in Fig. 3.

It is clear that when the films silica content increased to 15%mol, the strain initially decreased and then increased considerably. The decrease in strain implies a decrease in the lattice imperfections. Therefore, it is expected that adding 10-15%mol of SiO_2 into TiO_2 could improve some of its properties such as photocatalytic activity. This has been reported in some previous relevant literature [12, 24-25]. Further addition of silica caused the residual strain to increase.

3. 2. Morphological studies
The SEM micrographs of the surface of silica-embedded titania films heat-treated at 750°C are shown in Fig. 4. The quality of the thin films prepared on the substrate was uniform and homogeneous. The films exhibited a granular structure and were composed of

monodispersed uniformly distributed globular particles. It can be clearly seen that the particle size of the TiO_2–SiO_2 coatings considerably varied with the presence and the amount of SiO_2. In the case of the thin film which consisted of only TiO_2 (Fig. 4a), the particle size of the TiO_2 crystal was about 50-60 nm. However, the particle size of the TiO_2–SiO_2 crystal decreased as the silica percentage in the thin films increased. For example, the particle size of TiO_2–SiO_2 crystal was as small as about

30 nm in the film in which 15% mol SiO_2 was added (Fig. 4d). It seems that SiO_2 prevented the contact between TiO_2 particles and, as a consequence, obviously small particles were observed as compared to the pure TiO_2 coating. In addition, the surface of the films became smoother with the increase in the silica content of the films. By adding up to 15% mol of SiO_2, the films turned to a more agglomerated state so that the surface of these films became rougher.
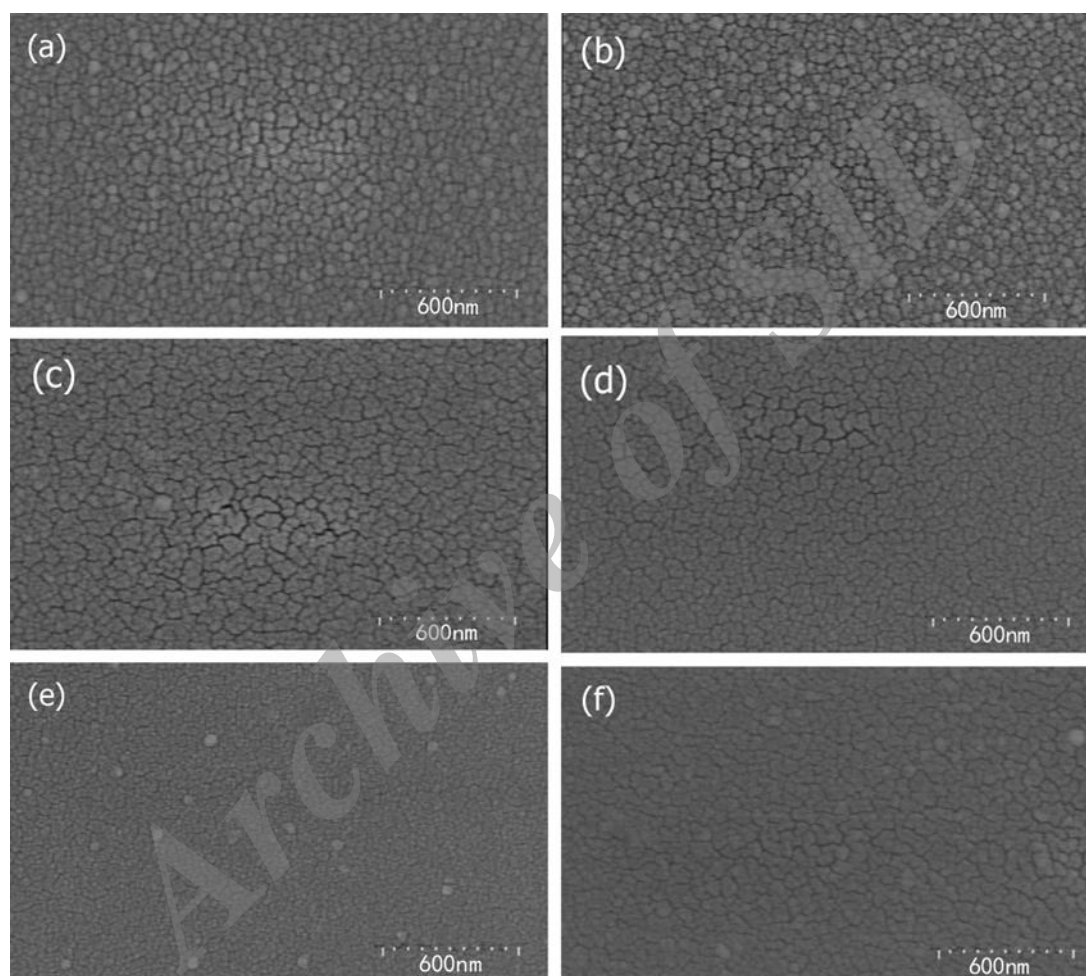

Fig. 4. The SEM micrographs of the surface of silica-embedded titania films heat-treated at 750°C: **(a):** TiO_2, **(b):** TiO_2-5% mol SiO_2, **(c):** TiO_2-10% mol SiO_2, **(d):** TiO2-15% mol SiO_2, **(e):** TiO_2-20% mol SiO_2, **(f):** TiO2-25% mol SiO_2

Fig. 5 shows the AFM images of the films with a granular structure consisting of interconnected grain particles fused together. It can be seen that the surface of the films became smoother with the addition of SiO_2 into TiO_2

which is in agreement with the results of the SEM studies. Although the morphologies of the silica-containing films were similar, their factors of surface roughness, represented by a root mean square (RMS), were different. The

dependence of the RMS roughness of the films on the silica content is shown in Fig. 6. As is evident in Fig.6, the minimum RMS, 0.916, belonged to the TiO_2–SiO_2 nanocomposite film that contained 10%mol of silica. The RMS of the surface of the films increased with the addition of up to 10%mol of SiO_2, indicating that the addition of suitable amount of SiO_2 to the TiO_2 film could help to improve the surface quality. Some literature works aimed at investigating the hydrophilic properties of the TiO_2–SiO_2 film confirmed that the addition of 10-15%mol of SiO_2 improves the surface superhydrophilicity [12, 26].
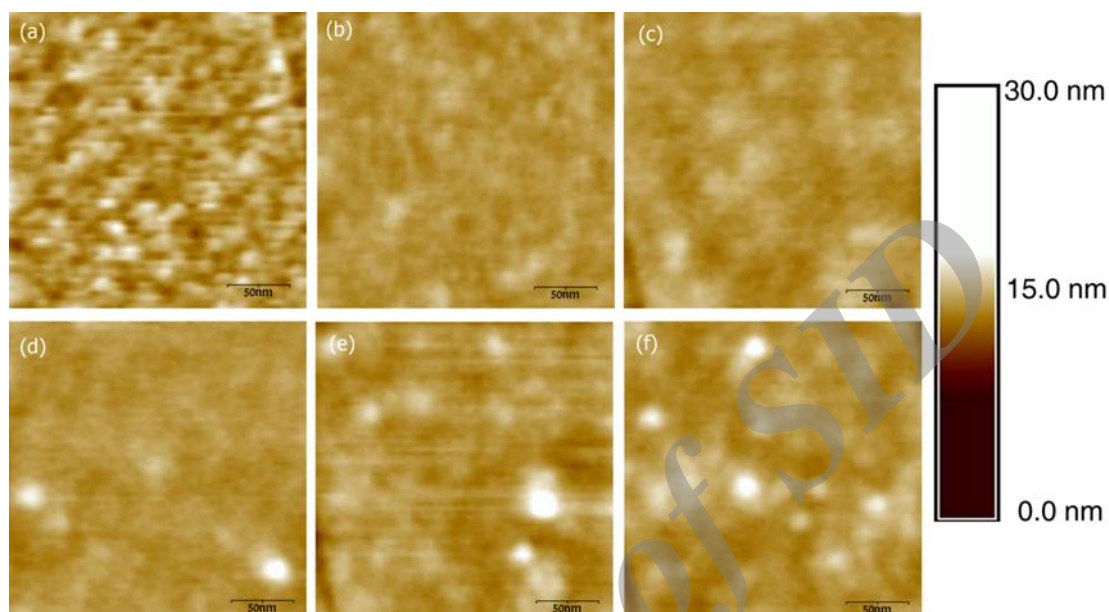

Fig. 5. AFM images of the surface of silica-embedded titania films heat-treated at 750°C, **(a), (b):** TiO_2-5%mol SiO_2, **(c):** TiO_2-10%mol SiO_2, **(d):** $TiO2$-15%mol SiO_2, **(e):** TiO_2-20%mol SiO_2, **(f):** TiO_2-25%mol SiO_2
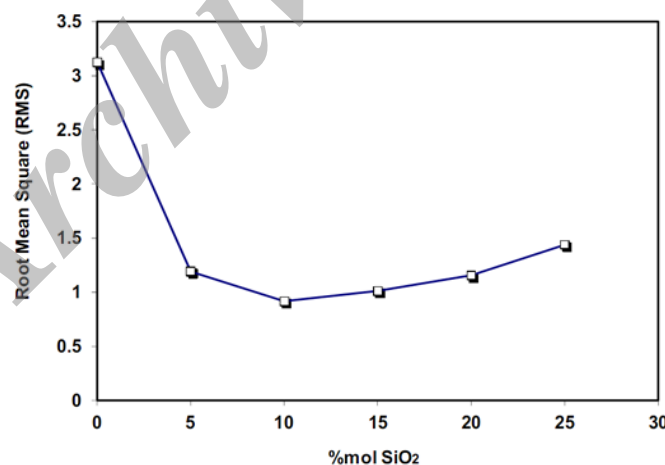

Fig. 6. The dependence of the RMS roughness of the films on the silica content

3. 3. Mechanical properties
Fig. 7a shows the hardness values determined by nanoindentation of the coatings as a function of the silica percentage of the coatings.

According to Fig. 7a, the hardness of the composite coatings decreased as the SiO2 content increased up to 5% mol and, consequently, it substantially enhanced the
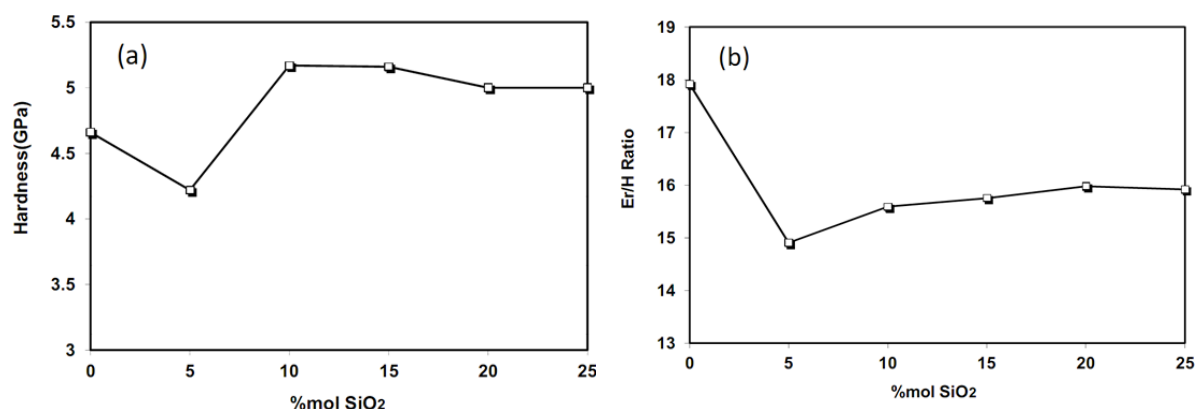
Fig. 7. (a): The hardness values and **(b):** the Er/H ratio of the films as a function of the silica percentage of the coatings
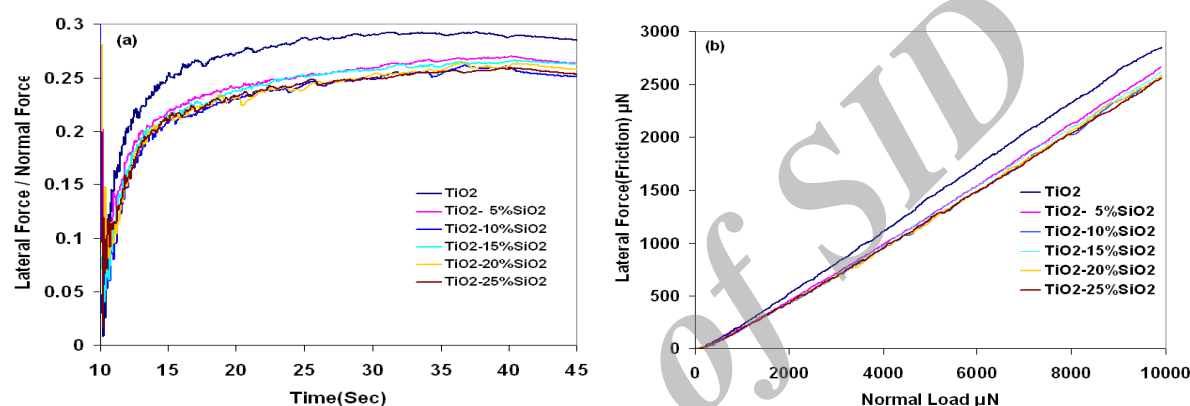

Fig. 8. (a): Changes in the friction coefficient (LF/NF) of the TiO2- SiO2 films containing 0-25%mol of SiO2 vs. time, **(b):** comparison of the friction force vs. the load curves measured during the microscratch test of the specimens

hardness of the composite coatings. The maximum hardness of TiO_2–SiO_2, ~ 5.2 GPa, belonged to the film which contained 10%mol of silica. In the case of exceeding 10%mol of SiO_2, the coating hardness appeared to slightly drop and then remained constant.

In Fig. 7b, the ratio of the measured reduced modulus to hardness E_r/H for each specimen is plotted against the silica content of the films. The E_r/H ratio is a criterion of the plastic index of the materials, and a small ratio supports elastic deformation during contact motion and is therefore beneficial for enhancing the tribological performance of the material [27-28]. According to Fig. 7b, adding silica into TiO_2 reduced the E_r/H ratio of the films and therefore it is expected to reveal much enhanced tribological performance.

Changes in the friction coefficient (LF/NF) of the TiO_2–SiO_2 films containing 0-25%mol of SiO2 vs. time are depicted in Fig. 8a. As can be seen, the pure TiO_2 film had the maximum friction coefficient, i.e. ~ 0.3. The addition of SiO_2 resulted in the loss of friction coefficient, so that this value would be ~ 0.25 for the films containing 20-25%mol of silica.

Fig. 8b compares the friction force vs. the load curves measured during the micro-scratch test of the specimens. It can be seen that the friction force measured from the Nano composite coatings was much lower than that of the pure TiO_2 coating across the load range, demonstrating the improved frictional properties of the coatings. It is worth noting that these results are in agreement with the AFM and SEM investigations and the obtained RMS values. On the other hand, the adhesive
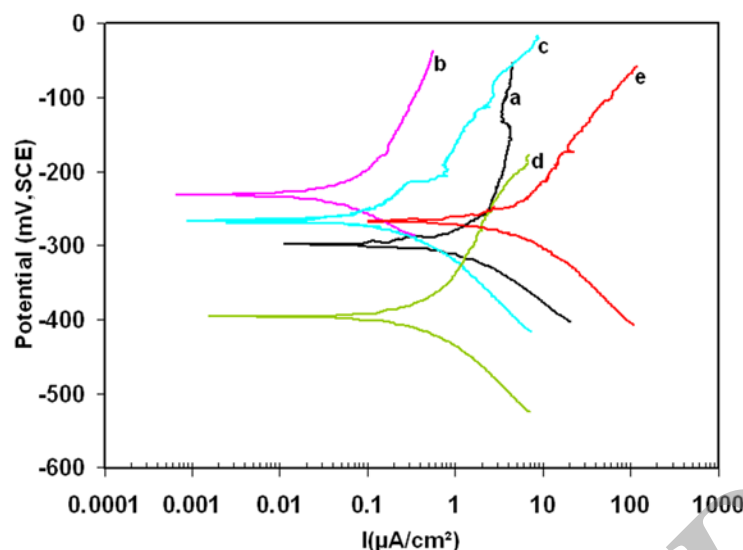
Fig. 9. The potentiodynamic polarization curves for: **(a):** 316L stainless steel, **(b):** TiO2, **(c):** TiO2-5%mol SiO2, **(d):** TiO2-15%mol SiO2, **(e):** TiO2-25%mol of SiO2 in 3%wt NaCl solutions

strength of the coating to the substrate remarkably increased after the addition of SiO_2 as the coating did not show adhesive failure even for loads up to 10000 μN applied in the test. The adhesion enhancement could be attributed to the interdiffused zone between the TiO_2–SiO_2 coatings and the stainless steel substrate as the interfacial region is expected to play an important role in the enhancement of the adhesive strength [29-30].

3. 4. Corrosion behavior of the coatings
The potentiodynamic polarization curves of the stainless steel substrate and the TiO_2 coatings containing 0, 5, 15 and 25%mol of SiO_2 in 3%wt NaCl solutions are shown in Fig. 9.
The comparison of the electrochemical behaviors of the uncoated substrate curve (a) and the pure TiO_2 film curve (b) indicated that the obtained potential values from the pure TiO_2 film revealed nobler values than those from AISI 316L. So, the stainless substrate will be corroded and pitted if the coating cracks due to the expansion coefficient difference between the stainless steel substrate and the coating. After adding up to 15%mol of SiO_2, the corresponding curves shifted toward more negative values (c, d) and then the potentials increased to nobler values (e). Among these potentiodynamic polarization curves, the electrochemical behavior of the TiO_2–SiO_2 film

which contained 15%mol of SiO_2 was different from the others. The corrosion potential of the stainless steel 316L was nobler than the open circuit potential (OCP) of TiO_2–15%mol SiO_2 film. As a result, the TiO_2–15%mol SiO_2 film was polarized as an anode. This behavior was similar to that of sacrificial anodes such as zinc in cathodic protection systems for metals. Unlike sacrificial anodes in corrosion system, this film could theoretically act as a non-sacrificial anode because the anodic reaction of this coating (d) was not passivation or the decomposition of the film itself; rather, it was the oxidation of water (H_2O) and/or adsorbed organic species by the photo-generated holes in the valence band of the TiO_2–SiO_2 film which can be called photocathodic protection effect of the TiO_2 family semiconductor. As noted before, TiO_2 as a semiconductor under normal conditions absorbs light and produces photo-generated electrons and holes. The photo-generated holes react with water to produce hydroxyl (OH-) radicals. So, hydroxyl ions act as hole traps that prevent electron–hole recombination. The increase in surface hydroxyl group can improve the photocatalytic activity of the films. It is well known that a surface with improved acidity can react with water to produce hydroxyl (OH-) radicals. It is shown that many binary metal oxides such as the TiO_2–SiO_2 composites show highly acidic
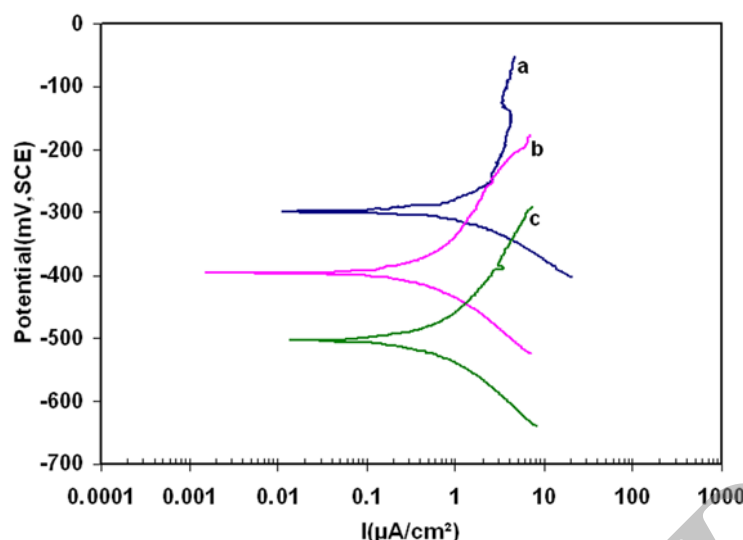
Fig. 10. The potentiodynamic polarization curves for: **(a):** the 316L stainless steel 316L electrode, and TiO_2-15%mol SiO_2 film before **(b):** and after **(c):** UV illuminations in 3%wt NaCl solutions

properties. It has been found that the high acidic strength of TiO_2–SiO_2 composites is attributable to the acidity of Ti–O–Si bonds [31]. So, the composite surface can adsorb more hydroxyl radicals than the pure TiO2 surface [32]. Given the foregoing results, by adding SiO_2 to TiO_2 thin films the photoactivity of the composite should be better than that of pure TiO_2.

Fig. 10 shows the potentiodynamic polarization curves for the TiO_2–SiO_2 film which contained 15%mol of SiO_2 before and after the UV illuminations and for a stainless steel 316L electrode in 3%wt NaCl solutions.

When the UV lamp was turned on, the OCP was shifted to −503 mV (SCE) and the anodic polarization was dramatically facilitated. Higher photoactivity of silica-embedding titania compared with the pure TiO_2 is brought about by higher heat treatment in the absence of rutile phase formation which results in the production of the anatase phase of high crystallinity and effectively reduces the bulk defects which serve as the recombination centers [24].

4. Conclusion

1. In the present research, the thin films in which SiO_2 was added to TiO_2 were deposited on AISI 316L stainless steel, and the effect of the added amount of SiO_2 on the films morphology and its mechanical properties and corrosion behavior of 316L stainless steel substrate were studied.

2. It was observed that the addition of a proper amount of SiO_2 to the TiO_2 film not only caused the particle size of TiO_2–SiO_2 crystal to decrease but also could help improve the surface quality.

3. The minimum RMS value was obtained from the film with a silica content of 10%mol.

4. Mechanical and tribological properties of the films were improved in the range of 10–15%mol of SiO_2 addition as compared to pure TiO_2.

5. By increasing the content of SiO_2, the minimum plastic index (Er/H ratio) and residual tensile strain were observed in the films with a silica content of 5 and 15 %mol, respectively.

6. The corrosion behavior of the 316L stainless steel was improved by adding 15%mol of SiO_2 not only for irradiated film but also for the film that was kept in darkness.

7. Under the UV illumination conditions, photo-generated electrons were quickly accumulated in this film compared with the film kept in darkness resulting in more negative shift of the OCP of the film and thus the substrate was perfectly protected by the film photocathodically.

References

1. G. X. Shen, Y. C. Chen and C. J. Lin, Corrosion protection of 316 L stainless steel by a TiO_2 nanoparticle coating prepared by sol–gel method, Thin Solid Films, Vol. 489, 2005, pp. 130.

2. M. Lia, S. Luo, P. Wu and J. Shen, Photocathodic protection effect of TiO2 films for carbon steel in 3% NaCl solutions, Electrochim. Acta, Vol. 50, 2005, pp. 3401.

3. Z. Liu, Y. Dong, Z. Chu, Y. Yang, Y. Li and D. Yan, Corrosion behavior of plasma sprayed ceramic and metallic coatings on carbon steel in simulated seawater, Mater. Design, Vol. 52, 2013, pp. 630.

4. D. S. R. Krishna, Y. Sun and Z. Chen, Magnetron sputtered TiO_2 films on a stainless steel substrate: Selective rutile phase formation and its tribological and anti-corrosion performance, Thin Solid Films, Vol. 519, 2011, pp. 4860.

5. S. M. Madani, M. Ehteshamzadeh and H. H. Rafsanjani, Investigation of the microstructure and corrosion performance of a nanostructured titania-containing hybrid silicate film on mild steel, Thin Solid Films, Vol. 519, 2010, pp. 145.

6. T. K. Rout, N. Bandyopadhyay, R. Narayan, N. Rani and D. K. Sengupta, Performance of titania–silica composite coating on interstitial-free steel sheet, Scripta Mater, Vol. 58, 2008, pp. 473.

7. S. Vives and C. Meunier, Mixed SiO_2–TiO_2 (1:1) sol–gel films on mild steel substrates: Sol composition and thermal treatment effects, Surf. & Coat. Tech, Vol. 202, 2008, pp. 2374.

8. T. Cetinkaya, L. Neuwirthová, K. Kutláková, V. Tomásek and H. Akbulut, Synthesis of nanostructured TiO_2/SiO_2 as an effective photocatalyst for degradation of acid orange, Appl. Surf. Sci, Vol. 279, 2013, pp. 384.

9. C. Beck, T. Mallat, T. Bu¨rgi and A. Baiker, Nature of Active Sites in Sol–Gel TiO_2–SiO_2 Epoxidation Catalysts, J. Catal, Vol. 204, 2001, pp. 428.

10. S. M. Jung, P. Grange, TiO_2–SiO_2 mixed oxide modified with H2SO$_4$: II. Acid properties and their SCR reactivity, Appl. Catal. A-Gen. Vol. 228, 2002, pp. 65.

11. J. Wang, C. Lua and J. Xiong, Self-cleaning and depollution of fiber reinforced cement materials modified by neutral TiO_2/SiO_2 hydrosol photoactive coatings, Appl. Surf. Sci., Vol. 298, 2014, pp. 19.

12. B. S. Boroujeny, A. Afshar v and A. Dolati, Photoactive and self-cleaning TiO_2–SiO_2 thin films on 316L stainless steel, Thin Solid Films, Vol. 520, 2012, pp. 6355.

13. D. Zhu and T. Kosugi, Thermal conductivity of GeO$_2$/SiO_2 and TiO_2/SiO_2 mixed glasses, J. Non-Cryst. Solids, Vol. 202, 1996, pp. 88.

14. M. Aizawa, Y. Nosaka and N. Fujii, Preparation of TiO_2/SiO_2 glass via sol-gel process containing a large amount of chlorine, J. Non-Cryst. Solids, Vol. 168, 1994, pp. 49.

15. X. Gao and I. E. Wachs, Titania–silica as catalysts: molecular structural characteristics and physico-chemical properties, Catal. Today, Vol. 51, 1999, pp. 233.

16. M. Fini, N. N. Aldini, P. Torricelli, G. Giavaresi, V. Borsari, H. Lenger, J. Bernauer, R. Giardino, R. Chiesa and A. Cigada, A new austenitic stainless steel with negligible nickel content: an in vitro and in vivo comparative investigation, Biomaterials, Vol. 24, 2003, pp. 4929.

17. J. A. Disegi and L. Eschbach, Stainless steel in bone surgery, Injury, Vol. 31, 2000, pp. D2.

18. Fujishima, T. N. Rao and D. A. Tryk, Titanium dioxide photocatalysis, J. Photochem. Photobiol. C, Vol. 1, 2000, pp. 1.

19. G. Lassaletta, A. Fernandez, J. P. Espinos, A.R. Gonzalez, Spectroscopic characterization of quantum-sized TiO_2 supported on silica: influence of size and TiO_2-SiO_2 interface composition, J. Phys. Chem., Vol. 99, 1995, pp. 1484.

20. J. A. Mejias, V. M. Jimenez, G. Lassaletta, A. Fernandez, J. P. Espinos and A. R. Gonzalez, Interpretation of the Binding Energy and Auger Parameter Shifts Found by XPS for TiO_2 Supported on Different Surfaces, J. Phys. Chem, Vol. 100, 1996, pp. 16255.

21. W. C. Oliver and G. M. Pharr, An improved technique for determining hardness and elastic modulus using load and displacement sensing indentation experiments, J. Mater. Res, Vol. 7, 1992, pp. 1564.

22. H. Tang, F. Levy, H. Berger and P. E. Schmid, Urbach tail of anatase TiO_2, Phys. Rev, Vol. 52, 1995, pp. 7771.

23. B. D. Cullity, Elements of X-ray Diffraction, Wesley Pub, Note Dame, 1978.

24. K. Y. Jung and S. B. Park, Anatase-phase titania: preparation by embedding silica and photocatalytic activity for the decomposition of trichloroethylene, J. Photochem. Photobiol. A: Chem, Vol. 127, 1999, pp. 117.

25. G. Xu, Z. Zheng, Y. Wu and N. Feng, Effect of silica on the microstructure and photocatalytic properties of titania, Ceram. Int., Vol. 35, 2009, pp. 1.

26.

27. M. Machida, K. Norimoto, T. Watanabe, K. Hashimoto and A. Fujishima, The effect of SiO$_2$ addition in super-hydrophilic property of TiO$_2$ photocatalyst, J. Mater. Sci, Vol. 34, 1999, pp. 2569.

28. H. Dong and T. Bell, Designer surfaces for titanium components, Anti-Corros. Method M, Vol. 46, 1999, pp. 338.

29. Leyland and A. Matthews, On the significance of the H/E ratio in wear control: a nanocomposite coating approach to optimised tribological behavior, Wear, Vol. 246, 2000, pp. 1.

30. P. Evans, T. English, D. Hammond, M. E. Pemble and D. W. Sheel, The role of SiO$_2$ barrier layers in determining the structure and photocatalytic activity of TiO$_2$ films deposited on stainless steel, Appl. Catal. A-Gen, Vol. 321, 2007, pp. 140.

31. L. Bamoulid, F. Benoît-Marquié, L. Aries, A. Guenbour, A. B. Bachir, M. T. Maurette, F. Ansart and S. El Hajjaji, Investigations on composition and morphology of electrochemical conversion layer/titanium dioxide deposit on stainless steel, Surf. & Coat. Tech, Vol. 201, 2006, pp. 2791.

32. M. Itoh, H. Hattori and K. Tanabe, The acidic properties of TiO$_2$-SiO$_2$ and its catalytic activities for the amination of phenol, the hydration of ethylene and the isomerization of butane, J. Catal, Vol. 35, 1974, pp. 225.

33. M. Zhang, L. Shi, S. Yuan, Y. Zhao and J. Fang, Synthesis and photocatalytic properties of highly stable and neutral TiO$_2$/SiO$_2$ hydrosol, J. Colloid Interface Sci, Vol. 330, 2009, pp. 113.